Highly-Sensitive Microwave Sensors Based on Open Complementary Split Ring Resonators (OCSRRs) for Dielectric Characterization and Solute Concentration Measurement in Liquids

Paris Velez, Katia Grenier, Javier Mata-Contreras, David Dubuc, Ferran Martín

IEEE Access
Multidisciplinary | Rapid Review | Open Access Journal

Received July 4, 2018, accepted August 9, 2018, date of publication August 27, 2018, date of current version September 21, 2018.

Digital Object Identifier 10.1109/ACCESS.2018.2867077

Highly-Sensitive Microwave Sensors Based on Open Complementary Split Ring Resonators (OCSRRs) for Dielectric Characterization and Solute Concentration Measurement in Liquids

PARIS VÉLEZ[1], (Member, IEEE), KATIA GRENIER[2], (Member, IEEE), JAVIER MATA-CONTRERAS[3], DAVID DUBUC[2], (Member, IEEE), AND FERRAN MARTÍN[1], (Fellow, IEEE)

[1]GEMMA/CIMITEC , Departament d'Enginyeria Electrònica, Universitat Autònoma de Barcelona, 08193 Bellaterra, Spain
[2]Laboratory of Analysis and Architecture of Systems, National Scientific Research Center, Université de Toulouse, 31400 Toulouse, France
[3]Departamento de Ingeniería de Comunicaciones, Universidad de Málaga, 29010 Málaga, Spain

Corresponding author: Paris Velez (paris.velez@uab.cat)

This work was supported in part by MINECO-Spain under Projects TEC2013-40600-R and TEC2016-75650-R, in part by the Generalitat de Catalunya under Projects 2017SGR-1159 and TECSPR15-1-0050, and in part by FEDER funds. The work of F. Martín was supported by the Institució Catalana de Recerca i Estudis Avançats.

ABSTRACT Differential permittivity sensors based on a pair of uncoupled microstrip lines, each one loaded with an open complementary split ring resonator (OCSRR), are proposed in this paper. The sensing principle is based on the measurement of the cross-mode insertion loss, very sensitive to asymmetric loading. Thus, by loading one of the OCSRRs with the reference sample, and the other one with the sample under test (SUT), the difference in the complex permittivity between both samples generates an asymmetry that gives rise to mode conversion. From the measurement of the cross-mode transmission coefficient, the dielectric properties of the SUT can be determined, provided those of the reference sample are well known. It is shown that by adding fluidic channels on top of the OCSRRs, the proposed sensor is useful for the measurement of the complex dielectric constant of liquids, and experimental results in mixtures of ethanol and deionized (DI) water and methanol in DI water, as a function of the ethanol/methanol content, are provided. Due to the high sensitivity of the proposed differential sensor to detect small perturbations (asymmetries), the structure is also of interest for the accurate measurement of solute concentrations in liquid solutions. In this paper, the structure is applied to monitor sodium content in aqueous solutions, and it is found that sodium concentrations as small as 0.25 g/L can be resolved.

INDEX TERMS Microwave sensors, dielectric characterization, permittivity sensors, differential sensors, split ring resonators, microstrip technology.

I. INTRODUCTION

Electrically small resonators, such as split ring resonators (SRRs) [1] or complementary split ring resonators (CSRRs) [2], have been extensively used for sensing purposes [3]–[32]. The electromagnetic properties of these resonant particles, either isolated or coupled to a transmission line, are severely influenced by the medium surrounding such particles. Therefore, it is possible to use SRRs, CSRRs, or other electrically small particles inspired by them, for the measurement of material properties, particularly dielectric properties [3]–[9], [16], [28], [29]. To this end, it is necessary to bring the material under test (MUT) in close proximity, or in touch, to the resonant element (dielectric loading), and material properties are inferred from the

changes experienced by the electromagnetic response of the particles. Since the electromagnetic properties of electrically small resonators also depend on the proximity and relative orientation of external elements (e.g., a transmission line coupled to it), it follows that such resonators are also useful for the measurement of spatial variables [10], [17], [20]–[27].

The most extended and simple working principle in microwave sensors based on resonant elements is the variation in the resonance frequency, phase and/or quality factor caused by the variable to be sensed [3]–[9], [29], [30]. For instance, the dielectric properties of materials (complex permittivity) can be inferred from the notch depth and frequency variation experienced by a specifically designed transmission line loaded with the sensing resonant element, in turn loaded with the material or sample under test (SUT) [5], [8], [9], [29], [30]. This sensing method is simple, but it is subjected to potential drifts caused by environmental changes (temperature, humidity, etc.). To alleviate this limitation, differential sensors, or sensors where the output variable is invariant (or scarcely sensitive) to ambient conditions constitute a good solution. In this latter type of sensors, cross sensitivities to environmental factors are minimized since changes in ambient conditions are seen as common-mode stimulus (differential sensors), or directly have no effect on the output variable.

Sensors based on symmetry disruption are robust to changes in environmental conditions [18], [19]. The reason is that symmetry is not affected by ambient factors, provided the environmental variables such as temperature, humidity and pressure are homogeneous (invariant to position) at the scale of the resonant elements (typically few millimeters or less). There are two main types of sensors based on symmetry disruption: (i) those based on coupling modulation [17], [20]–[27], and (ii) those based on frequency splitting [10]–[16], [32].

In coupling modulation sensors, a transmission line is symmetrically loaded with a single symmetric resonator. If the symmetry plane of the resonator at the resonance frequency of interest (typically the fundamental resonance) is of different electromagnetic nature (electric or magnetic wall) than the symmetry plane of the line, coupling between the line and the resonator is prevented [17]–[19], and the structure is transparent (i.e., all-pass in the vicinity of resonance). Conversely, if symmetry is disrupted (e.g., by misalignment between line and resonator, or by an asymmetric or inhomogeneous dielectric loading), line-to-resonator coupling is activated, producing a notch in the transmission coefficient (with depth dependent on the level of asymmetry). The main limitation of coupling modulation sensors is related to the fact that the output variable is the notch depth, relatively sensitive to noise effects. Nevertheless, it has been demonstrated that by properly choosing the type and shape of resonant element, coupling modulation sensors can be applied to the accurate measurement of angular displacements and velocities [22]–[24], [27], [33].

Frequency splitting sensors combine the advantages of differential sensors and frequency variation sensors (small cross sensitivities to environmental factors and larger robustness against noise effects). Although these sensors are not true differential sensors (in the sense that they are not based on two independent sensors), their working principle is very similar [18], [19]. In brief, a transmission line is symmetrically loaded with a pair of identical resonators (not necessarily symmetric). If symmetry is preserved, and the resonant elements are coupled to the line, a single notch in the transmission coefficient arises. However, if symmetry is truncated (for instance, by loading each resonant element with different samples), frequency splitting, manifested by the presence of two notches, arises. The output variables in this case are the difference in the transmission zero frequencies and the difference in the notch depths. These sensors have been applied to the measurement of the complex dielectric constant in solids [11], [16] and liquids [31].

One of the main drawbacks of permittivity sensors implemented by means of resonator loaded lines (either based on frequency variation, frequency splitting or coupling modulation), is their limited capability to detect small changes between the reference sample and the SUT (resolution), intimately related to their sensitivity. In this paper, a new type of highly sensitive differential sensors based on pairs of uncoupled microstrip lines loaded with open complementary split ring resonators (OCSRRs) are presented. The sensing principle, first presented in [28], is based on the measurement of the cross-mode insertion loss, whose magnitude is directly related (and it is highly sensitive) to the perturbation level. These sensors are applied in this paper to the measurement of the complex dielectric constant of liquids and to the determination of solution concentration (particularly sodium) in liquids (deionized –DI– water).

Reference [28] was mainly focused on presenting the working principle of these OCSRR based differential sensors and their analysis. In this paper, we extend such analysis, and we present a true differential sensor for the measurement of liquid properties, by adding fluidic channels on top of the OCSRRs. The designed sensor is then applied to the characterization of the complex permittivity of mixtures of DI water and ethanol and DI water and methanol, as well as to the measurement of sodium concentration in aqueous solutions. Performance comparison between the proposed sensor and other similar sensors used for dielectric characterization of liquids is also carried out.

The paper is organized as follows. Section II is focused on the working principle of the proposed sensors, and the specific sensing structure (based on OCSRRs) is presented. The circuit model and its validation, as well as an analysis to estimate the effects of the circuit model parameters on the sensitivity, are also included in this section. In Section III, the high sensitivity of the sensor to detect small changes in solute concentrations (sodium) in aqueous solutions is reported. The use of the sensor for the determination of

the complex dielectric constants of liquids is illustrated in Section IV. A comparison to other approaches is reported in Section V. Finally, the main conclusions are highlighted in Section VI.

II. STRUCTURE OF THE PROPOSED SENSOR, WORKING PRINCIPLE, CIRCUIT MODEL, VALIDATION AND ANALYSIS

A. SENSOR STRUCTURE AND WORKING PRINCIPLE

The sensors under study, first reported in [28], consist of a pair of uncoupled lines (microstrip in this work) each one loaded with a resonant element. Both resonant elements must be identical, and the whole four-port sensing structure must be perfectly symmetric with regard to the axial plane, as depicted in Fig. 1. For dielectric characterization, the considered resonant elements must be highly sensitive to the complex dielectric constant of their surrounding medium, or material under test (liquids or liquid solutions in this study) loading the resonators. For this reason, OCSRRs have been chosen for the implementation of these sensors. OCSRRs exhibit a distributed capacitance [34], highly influenced by the permittivity of the liquid under test (LUT), as long as it is put in contact to the resonant element (eventually through a protecting film to avoid substrate absorption). Consequently, OCSRRs are good candidates in order to achieve sensors highly sensitive to dielectric loading, able to resolve small changes in the permittivity of the LUT.

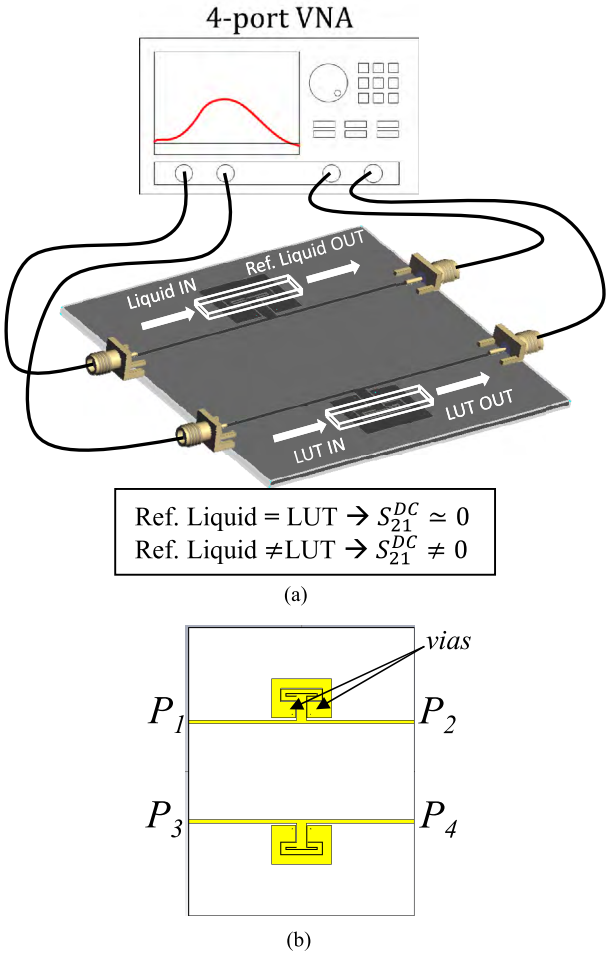

FIGURE 1. Sketch showing the working principle of the proposed sensor (a) and top view of the microwave part (i.e., the pair of OCSRR-loaded lines) (b). The metal surrounding the OCSRR is short-circuited to the ground plane through vias.

The working principle of the proposed differential sensor [see Fig. 1(a)] is mode conversion caused by asymmetry (when different liquids are added to the fluidic channels, necessary for OCSRR loading, see Fig. 2). If the channels are empty, symmetry is (ideally) preserved, and mode conversion is not possible. However, in a measurement operation (either to determine the solute concentration or the complex permittivity of the LUT), the reference liquid is added to the fluidic channel on top of one of the OCSRRs, whereas the LUT is injected to the channel on top of the other OCSRR. As long as both liquids, the reference liquid and the LUT, exhibit small (or large) differences, symmetry is truncated, and mode conversion arises. That is, any pure differential-mode signal injected to the input differential port is partially converted to the common mode in the output differential port, and vice versa. Hence, the cross-mode insertion loss, S_{21}^{DC}, a measurable quantity, must be indicative of the level of asymmetry, related to differences between the reference liquid and the LUT, and therefore it can be used as output variable for sensing purposes. The solute concentration is the input variable for this kind of measurements in LUTs with solute content, whereas for the measurement of the complex permittivity of liquids the input variables are the real and imaginary parts of the complex dielectric constant.

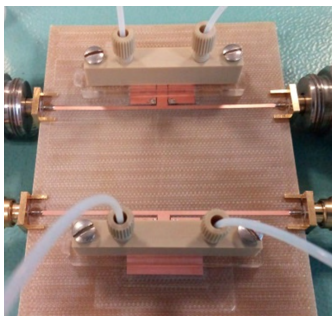

FIGURE 2. Photograph of the proposed sensor, including the fluidic channels and connectors.

The sensor has been implemented on the *FR4* substrate with thickness $h = 1.6$ mm, dielectric constant $\varepsilon_r = 4.4$ and loss tangent $\tan\delta = 0.02$. The uncoupled lines have a width and separation of 1.33 mm and 32 mm, respectively, corresponding to a characteristic impedance of $Z_c = 77\ \Omega$ for the single-ended, differential and common modes. The characteristic impedance has been chosen relatively high since this improves the sensitivity (to be discussed later). OCSRR dimensions are indicated in a zoom view for better comprehension in Fig. 3. The fluidic channels, made of polydimethylsiloxane (PDMS), are identical to those used

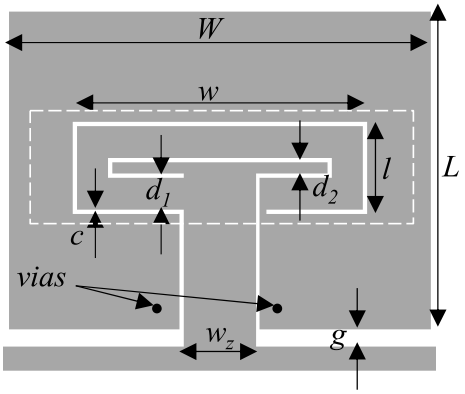

FIGURE 3. Zoom view of the OCSRRs. Dimensions are (in mm): $W = 20$, $L = 15.1$, $w = 14$, $l = 4.35$, $c = 0.2$, $d_1 = 1.5$, $d_2 = 0.55$, $g = 0.79$, $w_z = 3.4$ and $l_z = 6.49$. The radius of the vias is 0.1 mm. The channel limits are indicated by the dashed lines.

in [31]. Hence, the fabrication process is not reproduced here. Nevertheless, channel dimensions (including the dimensions of the mechanical parts) are given in Fig. 4 for completeness. Channels width is larger than l, the transverse dimension of the OCSRRs, so that the reference liquid and the liquid under test (LUT) are in contact with the whole OCSRR. Therefore, the channel position has little influence on the circuit model of Fig. 5, to be discussed next. The photograph of the sensor is shown in Fig. 2, where the capillaries for liquid injection can be appreciated. As in [31], a dry film of clear polyester (with dielectric constant 3.5 and thickness 55 μm) has been placed between the substrate and the fluidic channels in order to avoid liquid absorption by the substrate.

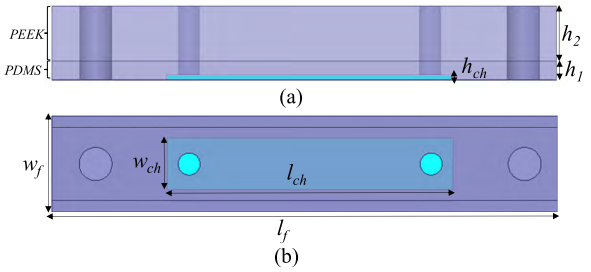

FIGURE 4. Lateral (a) and top (b) views of the fluidic channel, including the mechanical parts necessary for its attachment to the substrate. Channel dimensions are: $h_{ch} = 1.5$ mm, $l_{ch} = 26$ mm, $w_{ch} = 4.6$ mm; other relevant dimensions are $l_f = 46$ mm, $w_f = 12.6$ mm, $h_1 = 3$ mm, and $h_2 = 9$ mm.

B. CIRCUIT MODEL AND VALIDATION

The circuit model of the proposed sensor is depicted in Fig. 5. Note that this model is not symmetric, in order to account for the effects of the reference liquid and LUT, not necessarily identical in both channels. The pair of lines is described by transmission line sections (with impedance Z_c and electrical length kl) in the circuit schematic. For which concern the OCSRRs, such elements are modeled by lossy resonant tanks, connected to the respective host lines through inductances, L_z.

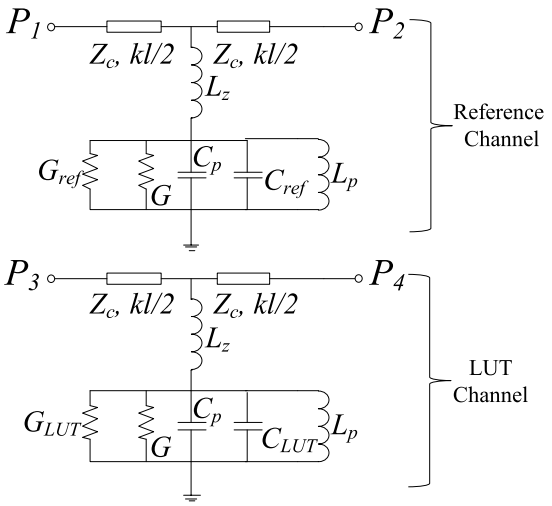

FIGURE 5. Circuit model of the proposed sensor.

Such inductances are not influenced by the presence of liquids in both channels. This also extends to the inductances of the resonant tanks, L_p. However, the capacitance and conductance of the OCSRRs depend on the liquid on top of them. Thus, we have opted in this work to designate as C_p the OCSRR capacitance corresponding to the empty channel, whereas the effects of the liquid (reference or LUT) on the OCSRR capacitance are taken into account by parallel connecting a capacitance, C_{ref} and C_{LUT}, respectively in each channel, to C_p. Similarly, the conductance of the empty channels, G, is parallel connected to G_{ref} and G_{LUT} to include the effects of the reference liquid and LUT, respectively, in the conductance of the OCSRRs.

It is worth mentioning that the OCSRRs have been separated significantly from the host lines in order to avoid possible effects of PDMS material (necessary for channel implementation surrounding the OCSRR geometry) on transmission line characteristics (line impedance). This has forced us to implement an OCSRR topology with a long connecting strip between the inner metallic region of the OCSRR and the host line, thus providing an inductive effect, taken into account through L_z. Conversely, such inductance was not included in [28], where such strip was considered to be of negligible length, since the considered sensor was not equipped with fluidic channels.

For model validation, several scenarios have been considered. First of all, we have obtained the responses of the individual lines by considering empty channels (i.e., loaded with air), see Fig. 6. Such responses have been inferred from CST Microwave Studio (electromagnetic simulation) and by means of the Agilent PNA N5221A vector network analyzer (experimental data). Using the parameter extraction method reported in [34], we have obtained the circuit parameters of the equivalent circuit model of Fig. 5 (see Table 1), and the corresponding response (simulation of the circuit schematic) is also depicted in Fig. 6. The agreement is very good,

TABLE 1. Extracted element parameters of the equivalent circuit model.

Channel 1/ Channel 2	L_z (nH)	L_p (nH)	C_p (pF)	C_{ref} (pF)	C_{LUT} (pF)	G (mS)	G_{ref} (mS)	G_{LUT} (mS)
Air/Air	4.87	7.79	2.04	0	0	0.59	0	0
DI water/ DI water	4.87	7.79	2.04	2.4	2.4	0.59	0.28	0.28
DI water/ Na solution	4.87	7.79	2.04	2.4	2.52	0.59	0.28	3.03

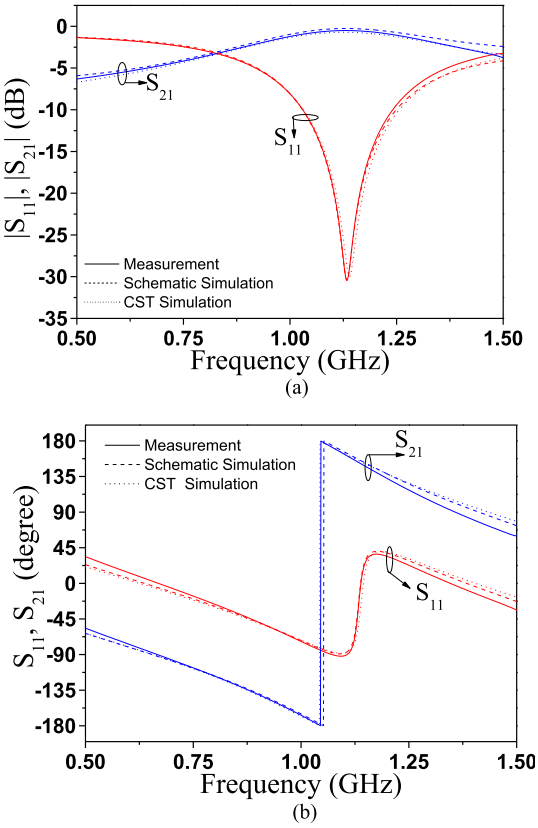

FIGURE 6. Insertion and return loss of the individual OCSRR-loaded line loaded with empty channel. (a) Magnitude response; (b) phase response.

pointing out the validity of the model for the description of the sensing structure, including the (empty) fluidic channels. The reference impedance of the ports has been considered to be $Z_0 = 50\ \Omega$.

In a second stage, we have injected deionized (DI) water in both channels, and the corresponding responses (identical for both OCSRR-loaded lines) are depicted in Fig. 7. The extracted parameters, also indicated in Table 1, have been used to obtain the response of the circuit schematic, which is in good agreement with the measured response. Therefore, it is confirmed that the presence of liquid in the channel modifies the capacitance and conductance of the corresponding OCSRR, but not the OCSRR and strip inductances, L_p and L_z.

The third validation experiment has been done by injecting DI water (reference liquid) in one channel and a solution of sodium in DI water (LUT), with a solute concentration of 20 g/L, in the other channel. The frequency responses of

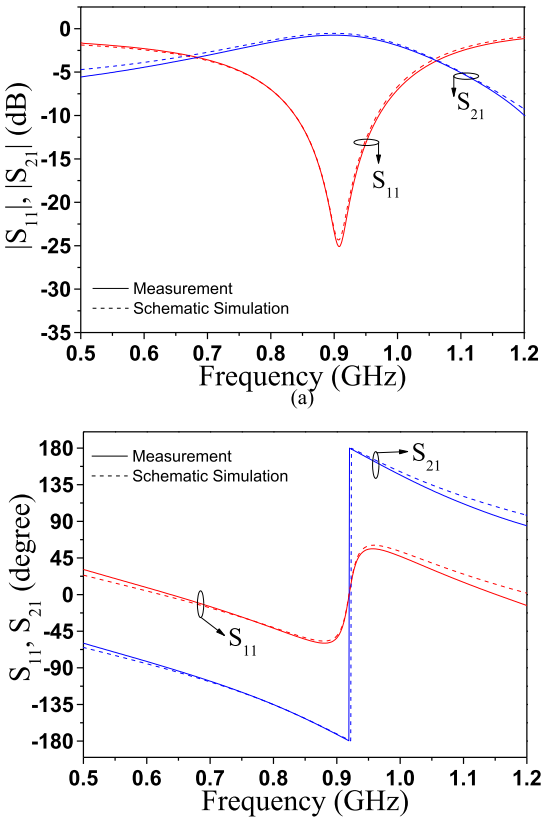

FIGURE 7. Insertion and return loss of the individual OCSRR-loaded line loaded with DI water in both channels. (a) Magnitude response; (b) phase response.

the OCSRR-loaded line with sodium solution in the channel are depicted in Fig. 8. Again, we have obtained the circuit parameters in this case (Table 1), and the corresponding circuit simulation, also included in Fig. 8, is in good agreement with the measured response. As can be seen, the presence of sodium does not modify significantly the capacitance of the OCSRR (as compared to the one of the OCSRR with DI water in the channel). However, the conductance is substantially altered (as revealed by the value of G_{LUT}). This means that the presence of this small quantity of sodium in DI water has small effect on the dielectric constant of the resulting solution, but significant effect on its loss tangent (or on the imaginary part of the complex permittivity), revealing a significant level of dielectric loss in DI water caused by the presence of sodium ions.

Finally, Fig. 9 depicts the cross-mode insertion, S_{21}^{DC}, and return, S_{11}^{DC}, loss measured in the last asymmetric loading case (DI water as reference liquid and the sodium solution as LUT). The same response inferred from the circuit model with extracted parameters (included in Table 1 for both lines, i.e., the one loaded with DI water and the one loaded with sodium solution) is also included in Fig. 9. Again, both responses are in good agreement.

With this set of experiments, the proposed circuit model is validated, and it is clear that the presence of liquid in the

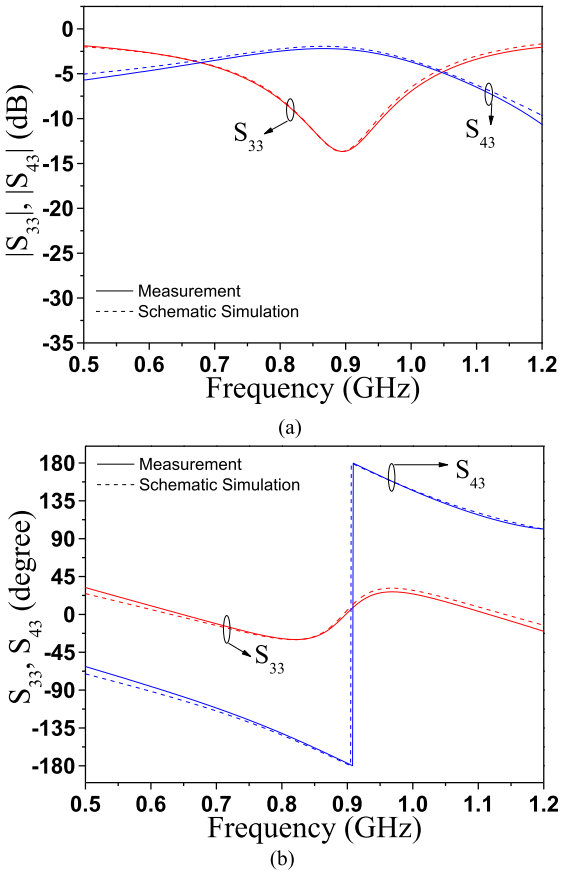

FIGURE 8. Insertion and return loss of the individual OCSRR-loaded line loaded with a solution of sodium in DI water in the channel. (a) Magnitude response; (b) phase response.

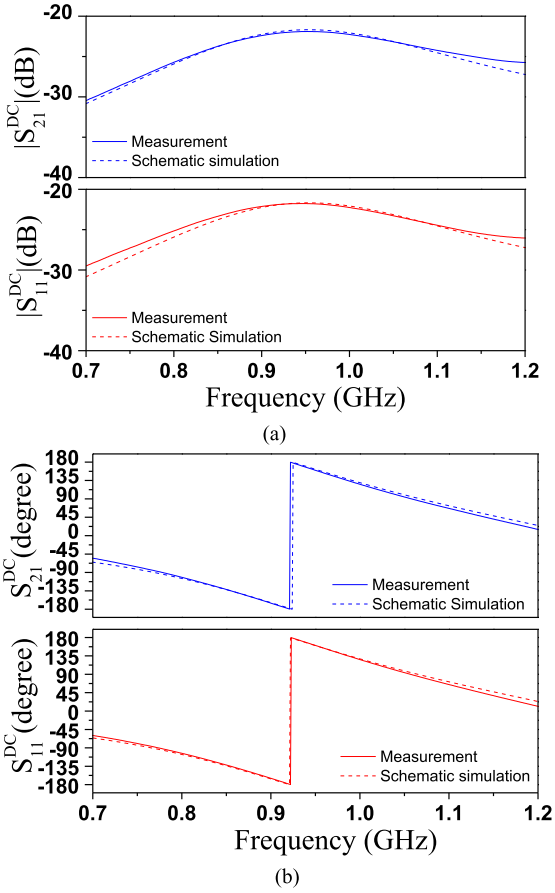

FIGURE 9. Cross-mode insertion and return loss of the sensor with DI water in the reference channel and a sodium solution in DI water in the LUT channel. (a) Magnitude response; (b) phase response.

channel has effect on the capacitance and conductance of the OCSRRs, leaving unaltered the inductive elements of the circuit model.

C. ANALYSIS

Once the circuit model of the proposed structure has been validated, let us use this model to analytically infer the influence of the different circuit elements on the cross-mode insertion loss. Note that, contrary to [28], in the model of Fig. 5, the inductive effect of the strip connecting the host lines to the central metallic regions of the OCSRRs, L_z, is considered. To simplify the analysis, we will assume that the lines are uncoupled and that the characteristic impedance of the host lines, Z_c, is set to the reference impedance of the ports (designated as Z_0, and typically 50 Ω), i.e., $Z_c = Z_0$. Under these conditions, the line sections of length $l/2$ only introduce a phase shift in the response of both lines, and we can neglect the effects of such line sections, as long as we are interested on the magnitude response of the cross-mode insertion loss. Note that this case is not the one considered in the reported sensors (with $Z_c = 77$ Ω in order to enhance sensitivity). Nevertheless, the following analysis provides useful guidelines for sensor design and sensitivity optimization.

If the lines are uncoupled, the cross-mode insertion loss is given by

$$S_{21}^{DC} = \frac{1}{2}\left(S_{21} - S_{43}\right) \tag{1}$$

where the transmission coefficients of the individual lines, neglecting the effects of the host line, are given by

$$S_{21} = \frac{1}{1 + \frac{Y_{ref}}{2} Z_0} \tag{2a}$$

$$S_{43} = \frac{1}{1 + \frac{Y_{LUT}}{2} Z_0} \tag{2b}$$

Y_{ref} and Y_{LUT} being the admittances of the shunt branches for the reference and LUT channels, respectively. Such admittances can be expressed as:

$$Y_{ref} = \frac{\frac{1}{L_p L_z}\left(\frac{1}{\omega_{ref}^2} - \frac{1}{\omega^2}\right) - j\frac{G'_{ref}}{L_z \omega}}{G'_{ref} + j\left\{\frac{\omega}{L_p}\left(\frac{1}{\omega_{ref}^2} - \frac{1}{\omega^2}\right) - \frac{1}{L_z \omega}\right\}} \tag{3a}$$

$$Y_{LUT} = \frac{\frac{1}{L_p L_z}\left(\frac{1}{\omega_{LUT}^2} - \frac{1}{\omega^2}\right) - j\frac{G'_{LUT}}{L_z \omega}}{G'_{LUT} + j\left\{\frac{\omega}{L_p}\left(\frac{1}{\omega_{LUT}^2} - \frac{1}{\omega^2}\right) - \frac{1}{L_z \omega}\right\}} \tag{3b}$$

where ω is the angular frequency, $G'_{ref} = G + G_{ref}$, $G'_{LUT} = G + G_{LUT}$, and ω_{ref} and ω_{LUT} are the angular frequencies of the parallel resonant tanks of the reference and LUT channels, respectively, i.e.,

$$\omega_{ref} = \frac{1}{\sqrt{L_p(C_p + C_{ref})}} \tag{4a}$$

$$\omega_{LUT} = \frac{1}{\sqrt{L_p(C_p + C_{LUT})}} \tag{4b}$$

Evaluating (3a) and (3b) at ω_{ref}, and introducing the results in 2(a) and 2(b), respectively, the results in 5(a) and 5(b) are obtained, where $\omega_L^{-2} = L_p \cdot (C_{LUT} - C_{ref})$, and $S_{21,\omega_{ref}}$ and $S_{43,\omega_{ref}}$ are the transmission coefficients of the reference channel line and LUT channel line, respectively, evaluated at ω_{ref}.

$$S_{21,\omega_{ref}} = \frac{1}{1 - \frac{\frac{Z_0 G'_{ref}}{L_z \omega_{ref}}\left(jG'_{ref} - \frac{1}{L_z \omega_{ref}}\right)}{2\left(G'^2_{ref} + \frac{1}{L_z^2 \omega_{ref}^2}\right)}} \tag{5a}$$

Despite the fact that liquids exhibit non-negligible values of the loss tangent (as compared to those of good dielectrics), it is reasonable to assume that losses are small, i.e., G'_{ref} and G'_{LUT} are small. This hypothesis is reasonable even for liquid solutions containing ions, if their concentration is small. Let us now consider that the reference liquid and the LUT exhibit similar dielectric constants, a reasonable hypothesis in situations where the LUT is a diluted solution of the reference liquid (the situation studied in Section III). Under these approximations (low-losses and small perturbations), the right hand side of the denominator of (5a) and (5b) is small [See (5b), as shown at the bottom of this page], and consequently signal transmission in both channels at ω_{ref} is roughly total. Thus, using the approximation $1/(1-x) = 1+x$, valid for small values of x [as occurs in expressions (5a) and (5b)], and taking into account that for small perturbations ($C_{LUT} \approx C_{ref}$) and low-losses (G'_{ref} and G'_{LUT} small), the following approximations hold

$$\frac{\omega_{ref}^2 L_z}{\omega_L^2 L_p} \ll 1 \tag{6}$$

$$G'^2_{ref} L_z^2 \omega_{ref}^2 \ll 1; \quad G'^2_{LUT} L_z^2 \omega_{ref}^2 \ll 1, \tag{7}$$

the real and the imaginary parts of the cross-mode insertion loss can be expressed as:

$$\mathrm{Re}\left\{S^{DC}_{21,\omega_{ref}}\right\} = \frac{Z_0}{4}\left[G_{LUT} - G_{ref} + G'_{ref} L_z (C_{LUT} - C_{ref})\omega_{ref}^2\right] \tag{8a}$$

$$\mathrm{Im}\left\{S^{DC}_{21,\omega_{ref}}\right\} = \frac{Z_0 \omega_{ref}}{4}\left[C_{LUT} - C_{ref} + L_z(G'^2_{ref} - G'^2_{LUT})\right] \tag{8b}$$

and

$$\left|S^{DC}_{21,\omega_{ref}}\right| = \sqrt{\left(\mathrm{Re}\left\{S^{DC}_{21,\omega_{ref}}\right\}\right)^2 + \left(\mathrm{Im}\left\{S^{DC}_{21,\omega_{ref}}\right\}\right)^2} \tag{9}$$

By comparing (8) with the cross-mode insertion loss obtained in [28], it can be appreciated that the terms proportional to L_z are not present in [28], where L_z was neglected due to the small considered distance between the host lines and the OCSRRs. Note, however, that a second order term is included in [28]. The reason is that in that work, a second-order Taylor expansion was considered, but such second order term is very small as compared to the first order terms, and, consequently, it can be neglected. If the terms dependent on L_z in expressions (8) cannot be neglected, the sensitivity of the cross-mode insertion loss to variations in the complex dielectric constant of the LUT (as compared to the reference liquid and manifested as variations in the capacitance and conductance of the resonant tanks) does not exhibit a simple dependence on the circuit parameters.

However, if L_z is sufficiently small and the corresponding terms can be neglected, the modulus of the cross-mode insertion loss is simply given by:

$$\left|S^{DC}_{21,\omega_{ref}}\right| = \frac{Z_0}{4}\sqrt{(G_{LUT} - G_{ref})^2 + \omega_{ref}^2 (C_{LUT} - C_{ref})^2} \tag{10}$$

from which it follows that the sensitivity of the cross-mode insertion loss (modulus) to the variation in the complex dielectric constant depends on the frequency of the resonant tank of the reference channel, ω_{ref}, and on the characteristic impedance of the host line, $Z_c = Z_0$ in the present study. However, ω_{ref} has small influence on the sensitivity of the cross-mode insertion loss to variations in the conductivity. Increasing ω_{ref} is convenient to enhance the sensitivity to dielectric constant variations, but at the expense of smaller OCSRR size. Nevertheless, under the considered approximations, the sensitivity does not depend on the particular values of the reactive elements of the circuit model, in particular those describing the sensing elements (OCSRRs). According to these results, rather than the shape of the OCSRRs, its resonance frequency (when it is loaded with the reference liquid) is the fundamental parameter determining the sensitivity to dielectric constant variation. Under the condition $Z_c = Z_0$, and assuming that Z_0 is not a design parameter, the sensitivity to the loss tangent variation cannot be controlled under the

$$S_{43,\omega_{ref}} = \frac{1}{1 - \frac{\frac{Z_0 G'_{LUT}}{L_z \omega_{ref}}\left[\frac{\omega_{ref}}{L_p \omega_L^2} - \frac{1}{L_z \omega_{ref}}\right] - \frac{Z_0 G'_{LUT}}{L_p L_z \omega_L^2} + j\left(\frac{Z_0}{L_z L_p \omega_L^2}\left[\frac{\omega_{ref}}{L_p \omega_L^2} - \frac{1}{L_z \omega_{ref}}\right] + \frac{Z_0 G'^2_{LUT}}{L_z \omega_{ref}}\right)}{2\left(G'^2_{LUT} + \left[\frac{\omega_{ref}}{L_p \omega_L^2} - \frac{1}{L_z \omega_{ref}}\right]^2\right)}} \tag{5b}$$

considered approximations. However, by relaxing this condition, i.e., by increasing Z_c, maintaining the value of Z_0 (i.e., $Z_c \neq Z_0$), the sensitivity increases, as it has been corroborated from electromagnetic simulations (Fig. 10). Note that for the considered reference liquid and LUT, indicated in the caption, the variation experienced by the cross-mode transmission coefficient increases with Z_c. For this reason, we have chosen $Z_c = 77\ \Omega$, larger than $Z_0 = 50\ \Omega$, in this work. The analysis in this case is not so simple, but for relatively small variations of Z_c with regard to Z_0, the effects of Z_c and ω_{ref} on S_{21}^{DC} are expected to be similar.

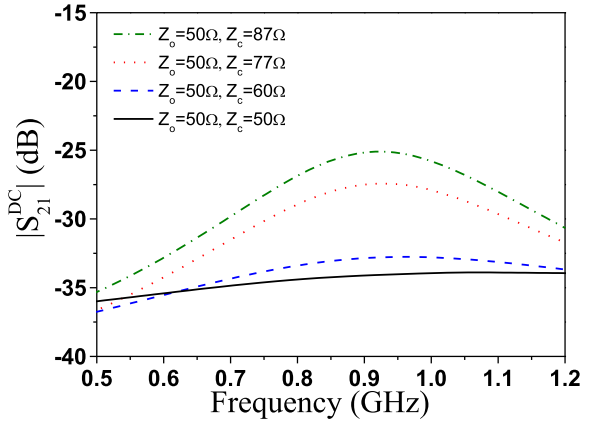

FIGURE 10. Effect of the value of the line impedance (Z_c) on the cross mode insertion loss. The simulations have been carried out by means of the *Ansys HFSS* electromagnetic simulator, by considering DI water as reference liquid (with complex dielectric constant $\varepsilon_{water} = \varepsilon' - j\varepsilon'' = 80.86 - j3.04$) and with the LUT channel containing a hypothetical liquid with real and imaginary parts of the complex dielectric constant 15% larger than those of DI water.

It should be clarified at this point that for solute concentration measurements (the objective of the next section), the input variable is the solute concentration, intimately related to the dielectric constant and loss tangent of the LUT (and consequently to C_{LUT} and G_{LUT}). Therefore, the effects of Z_0 and ω_{ref} on sensitivity, defined in this case as the derivative of $|S_{21}^{DC}|$ with the solute concentration, do also apply.

III. MEASURING SOLUTE CONCENTRATION IN DILUTED SOLUTIONS

Determining the solute content in diluted solutions requires highly sensitive techniques. The novel technique proposed in this work is based on measuring the magnitude of the cross mode insertion loss, highly sensitive to small perturbations in the LUT (solution) in comparison to the reference liquid (i.e., the solvent without solute), and consequently very useful in applications where solute concentrations are very small.

In this work, the study is focused on diluted solutions of sodium in DI water (LUT). Thus, the reference liquid is DI water (the solvent). We have obtained the cross-mode insertion loss corresponding to different levels of sodium concentration, between 0.25 g/L (the minimum level that can be reasonably resolved) and 80 g/L (the solutions have been prepared by carefully weighting the sodium content by means of a precision weighting machine, model *Rs-Pro*, with 1mg resolution). The results (in dB) are depicted in Fig. 11(a), where it can be appreciated that the cross-mode insertion loss experiences significant variations in the overall magnitude when the sodium concentration increases. Figure 11(b) depicts the dependence of the maximum value of $|S_{21}^{DC}|$ for each curve as a function of the sodium concentration. It can be seen that for small sodium concentrations, $|S_{21}^{DC}|_{\max}$ varies significantly with the sodium content, and such variation progressively decreases. Thus, the sensitivity is maximum for small concentrations and then it progressively decreases (Fig. 12). It is remarkable that the variation experienced by $|S_{21}^{DC}|_{\max}$ is approximately linear (and hence the sensitivity is roughly constant) up to sodium concentrations of 2.5 g/L, as it can be appreciated in the zoom view shown in the inset of Fig. 11(b). The maximum value of the sensitivity is $S = 0.0092(g/L)^{-1}$.

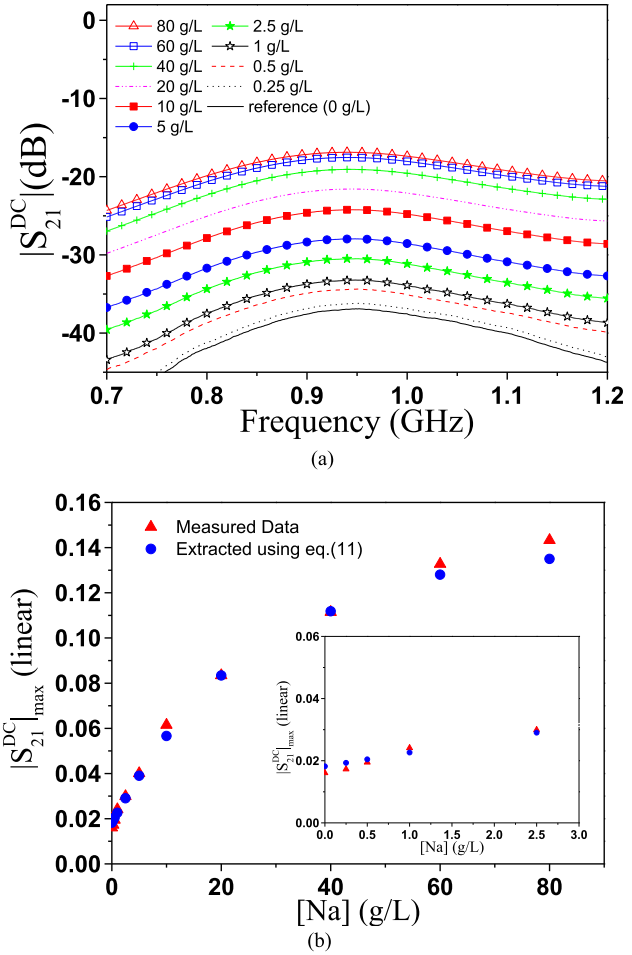

FIGURE 11. Effects of sodium concentration on the cross-mode insertion loss. (a) Dependence of the cross-mode insertion loss on frequency; (b) relation between sodium concentration and $|S_{21}^{DC}|_{\max}$ in linear form. The inset in (b) depicts a zoom view for small concentrations.

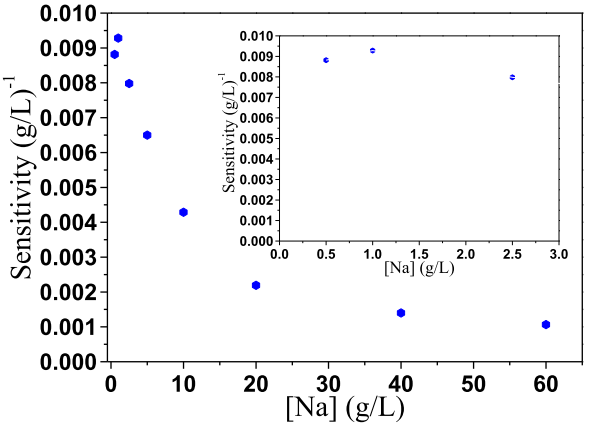

FIGURE 12. Sensitivity dependence on the sodium concentration.

From the results of Fig. 11(b), we have obtained the calibration curve, an order-3 polynomial, providing a correlation coefficient of $R^2 = 0.9983$, i.e.,

$$[Na](g/L) = 36807 \cdot \left|S_{21}^{DC}\right|_{\max}^{3} - 3480.1 \cdot \left|S_{21}^{DC}\right|_{\max}^{2} + 322.68 \cdot \left|S_{21}^{DC}\right|_{\max} - 4.76 \quad (11)$$

Note that the previous curve does not exactly predict a null concentration of sodium when $|S_{21}^{DC}|_{\max} = 0$. The reason is that when the LUT is pure DI water, i.e., without sodium content, the measured cross-mode insertion loss has a finite value [Fig. 11(a)]. Nevertheless, using the calibration curve, the sodium concentrations of unknown samples can be inferred with high accuracy, from the measurement of the cross-mode insertion loss. This aspect is confirmed from the small differences between the nominal values of sodium concentration, and the values provided by the calibration curve inferred from the measured values of $|S_{21}^{DC}|_{\max}$, also included in Fig. 11(b).

We would like also to mention that the method proposed for the measurement of sodium concentration in diluted aqueous solutions is able to resolve concentration levels as small as 0.25 g/L. This resolution is by far smaller than the typical levels of sodium concentration in blood plasma in adults (around 3.2 g/L). Therefore, these results point out the potential of the method for the detection of electrolytic imbalance in blood, caused by an excess or defect of electrolytes, such as sodium, potassium, calcium, magnesium, etc. The dominant component is sodium, but the presence of the other electrolytes in blood plasma is not negligible. However, these components are present in plasma as conductive ions, influencing severely the conductivity of plasma (and hence the imaginary part of the dielectric constant). Consequently, by comparing a blood sample (LUT) with blood with normal levels of electrolyte concentration (reference sample), it is expected that abnormal concentrations of electrolytes can be detected, if they are present in the LUT. The proposed approach is very sensitive to small differences in the LUT and reference sample, but it is worth mentioning that the main reason that explains the high sensitivity and resolution to detect small variations in sodium concentration is related to the fact that a small sodium density suffices to substantially modify the conductivity of DI water. Therefore, a small sodium content is expected to significantly alter the loss tangent, or the imaginary part of the dielectric constant, of DI water, resulting in significant mode conversion. However, from the comparison between Figs. 7(a) and 8(a), we can conclude that the presence of sodium does not significantly alter the real part of the dielectric constant, as results from the small variation of the resonance frequencies in those figures.

The measured responses of Fig. 11(8a) are referred to 50 Ω ports, i.e., $Z_0 = 50\ \Omega$. In order to validate the approximations in (9) and (10), from these results we have obtained S_{21}^{DC} referred to ports with impedance $Z_0 = Z_c = 77\ \Omega$ (using *Keysight ADS*), and we have obtained S_{21}^{DC} at ω_{ref} (Fig. 13). The results are compared to the prediction given by (9) and (10), and also to the exact analytical solution. It can be appreciated that the agreement between the measurement, the exact analytical solution and the approximate solution given by (9) is very good in the considered range of sodium concentrations. However, the rough approximation (10) is only valid for very small perturbations. The reason is that L_z is not very small in the considered sensing structure, and the influence of the terms that depend on L_z increase with sodium concentration. The results of Fig. 13 validate the analysis carried out in Section II.B, and point out the effects of circuit parameters on the cross-mode insertion loss at ω_{ref}. Note that in Fig. 11(b), the considered output variable is $|S_{21}^{DC}|_{\max}$, rather than $\left|S_{21,\omega_{ref}}^{DC}\right|$ (and the reference impedance of the ports is $Z_0 = 50\ \Omega$). Nevertheless, the responses of Fig. 11(a) exhibit a very soft dependence on frequency in the vicinity of ω_{ref}. Therefore, the conclusions derived at the end of Section II.B relative to the effects of model parameters on cross-mode insertion loss at ω_{ref}, can be extended to the output variable, $|S_{21}^{DC}|_{\max}$, even by considering the usual reference impedance of the ports, $Z_0 = 50\Omega$.

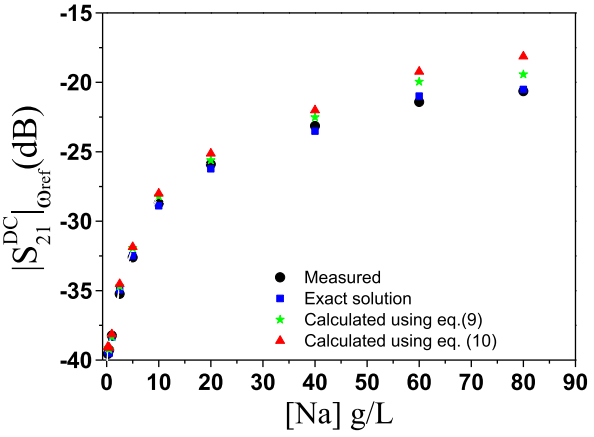

FIGURE 13. Variation of the cross-mode insertion loss at ω_{ref} as a function of sodium concentration. The considered port impedances are $Z_0 = 77\ \Omega$, as indicated in the text.

IV. MEASURING THE COMPLEX DIELECTRIC CONSTANT IN LIQUIDS

The sensor of Fig. 2 can also be used for dielectric characterization of liquids using the same principle. In this case, calibration curves inferred from mixtures of DI water and ethanol are obtained. Since pure DI water and pure ethanol exhibit complex dielectric constants of $\varepsilon_{water} = \varepsilon' - j\varepsilon'' = 80.86 - j3.04$ and $\varepsilon_{ethanol} = \varepsilon' - j\varepsilon'' = 27.86 - j9.79$, respectively (at ω_{ref}), it follows that the method is especially suitable for dielectric characterization of liquids with complex dielectric constant within the previous ranges. After introducing DI water in the reference channel, we have then subsequently injected different mixtures of DI water and ethanol, with varying ethanol concentration, as LUT, and we have measured the S-parameters, including the cross-mode insertion loss, for each mixture. Figure 14 depicts the single-ended insertion and return loss corresponding to the line loaded with the LUT, as well as the cross-mode insertion loss. It can be seen that, as the ethanol content increases, absorption, due to losses, increases. This is an expected result provided the imaginary part of the dielectric constant in ethanol is larger than in DI water. However, the real part of the complex dielectric constant is smaller in ethanol, hence decreasing the capacitance contribution of the LUT when the ethanol content increases, and consequently shifting up the resonance frequency [see Fig. 14(b)].

It can be seen that the cross-mode insertion loss exhibits a large excursion by varying the ethanol concentration from 0% (pure DI water) to 100% (pure ethanol). For this reason, this parameter is used for the measurement of the complex dielectric constant of the LUT. Fig. 15 depicts the variation of $\Delta|S_{21}^{DC}|_{\max} = |S_{21}^{DC}|_{max\_Ref} - |S_{21}^{DC}|_{max\_LUT}$, as well as the variation of the frequency position of the maximum insertion loss, $\Delta f_{max} = f_{max\_Ref} - f_{max\_LUT}$, as a function of the ethanol concentration. Note that the sub-indexes *max_Ref* and *max_LUT* denote the maximum value of the cross-mode insertion loss and the corresponding frequency when the LUT channel is loaded with the reference liquid (symmetric case) and LUT, respectively. From these data, and from the knowledge of the complex dielectric constant of the different mixtures (given by the Weiner model [35], see Fig. 16), we have obtained the calibration curves for both the incremental real, $\Delta\varepsilon'$, and imaginary, $\Delta\varepsilon''$, parts of the dielectric constant, using multiple linear regression. Such curves are

$$\Delta\varepsilon' = k_{11}\Delta|S_{21}^{DC}|_{max} + k_{12}\Delta f_{max} \quad (12a)$$

$$\Delta\varepsilon'' = k_{21}\Delta|S_{21}^{DC}|_{max} + k_{22}\Delta f_{max} \quad (12b)$$

where the coefficients are those indicated in Table 2, and provide a correlation coefficient of $R^2 = 0.994$.

Using equations 12(a) and (b) and the data of Fig. 15, we have obtained the real and imaginary part of the complex dielectric constant for the different mixtures of ethanol in DI water (Fig. 16). The results are in good agreement with the prediction given by the Weiner model (the upper and lower limits of that model are also indicated in the figure). Indeed, such good agreement is expected provided the calibration curves have been obtained from the Weiner model applied to

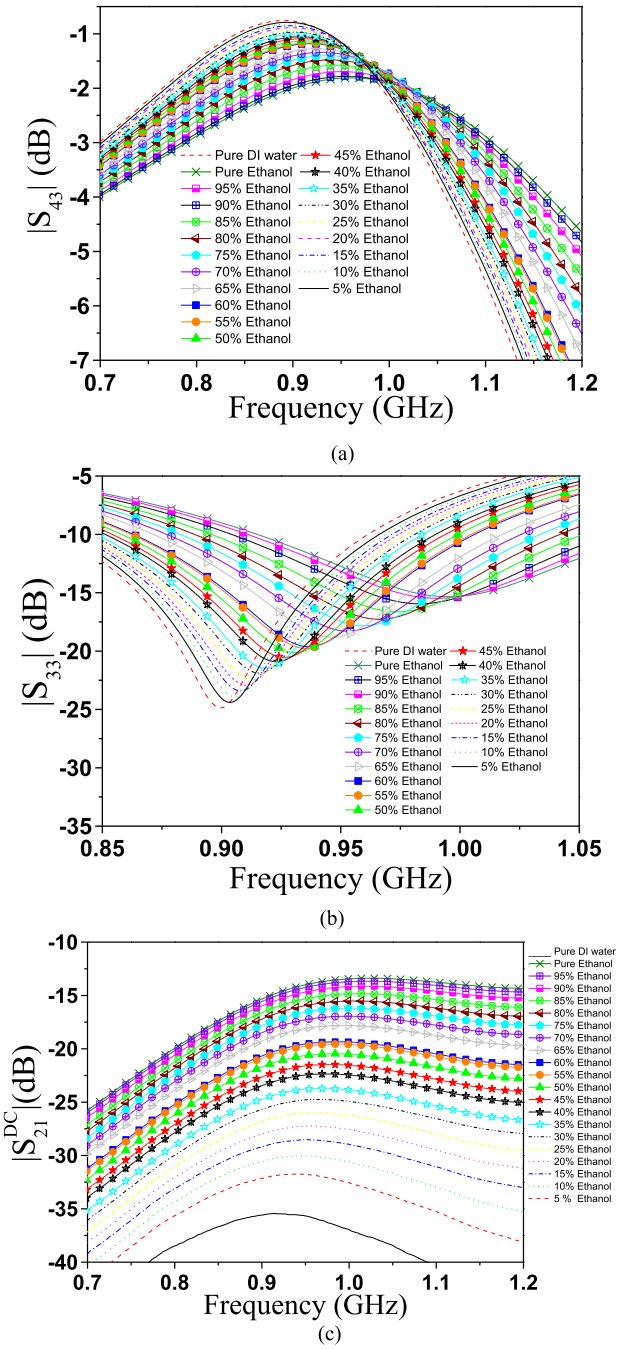

FIGURE 14. Measured insertion (a) and return (b) loss of the single-ended line loaded with different mixtures of DI water and ethanol, and cross-mode insertion loss (c).

TABLE 2. Coefficients of the calibration curves for $\Delta\varepsilon'$ and $\Delta\varepsilon''$ in DI water/ethanol mixtures.

k_{11} (dB^{-1})	k_{12} (MHz^{-1})	k_{21} (dB^{-1})	k_{22} (MHz^{-1})
-1.805	0.107	-0.092	-0.063

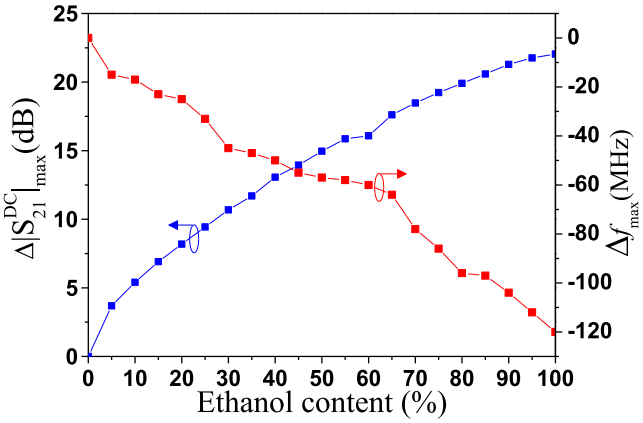

FIGURE 15. Dependence of $\Delta|S_{21}^{DC}|_{max}$ (in dB) and Δf_{max} with the ethanol content.

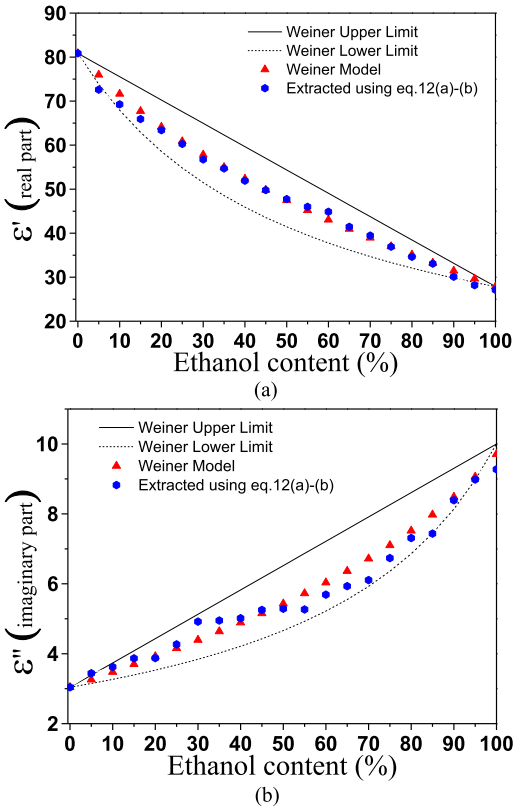

FIGURE 16. Extracted value for the real (a) and imaginary (b) parts of the complex dielectric constant in mixtures of DI water/ethanol. The static Weiner model is also included for comparison purposes.

ethanol/DI water mixtures. Nevertheless, to properly validate the functionality of the sensor, we have used the calibration curves to determine the complex dielectric constant in several mixtures of methanol in DI water. To this end, pure DI water has been injected to the reference channel, whereas different mixtures of DI water and methanol have been subsequently injected to the LUT channel by varying the methanol concentration (from 0% to 100% in steps of 5%). The cross-mode insertion loss for each measurement is plotted in Fig.17. From

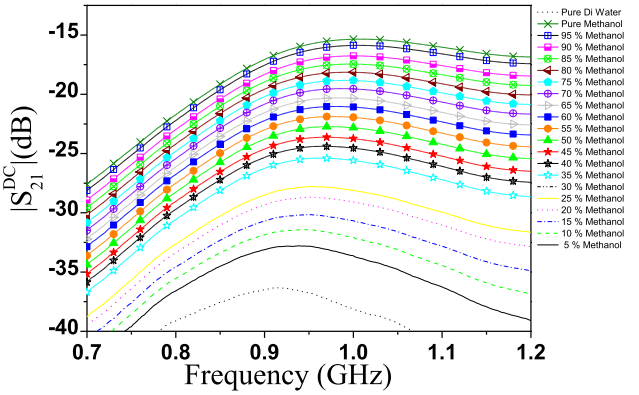

FIGURE 17. Measured cross-mode insertion loss corresponding to different mixtures of DI water and methanol.

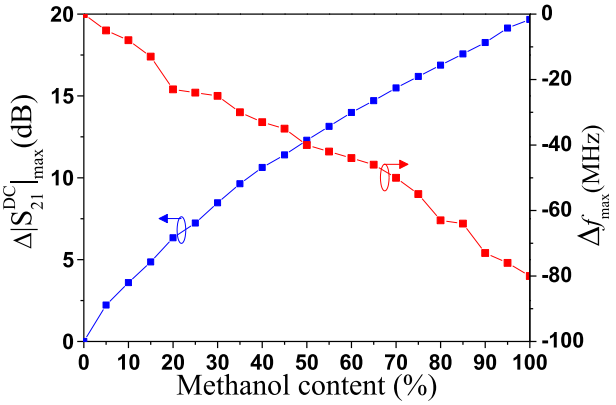

FIGURE 18. Dependence of $\Delta|S_{21}^{DC}|_{max}$ (in dB) and Δf_{max} with the methanol content.

the values of $\Delta|S_{21}^{DC}|_{\max}$ and Δf_{max} (depicted in Fig. 18), we have obtained the variation of the real and imaginary parts of the complex dielectric constant [using expressions 12(a) and (b)] for all the mixtures (with reference to the values of DI water, the reference liquid). The results are depicted in Fig. 19 and are compared to the predictions of the Weiner model. The good agreement is indicative of the validity of the proposed sensor to determine the complex dielectric constant of liquids. In particular, the nominal complex dielectric constant of methanol at the frequency of sensor operation, i.e., 30.87− j6.48, is reasonably predicted.

V. COMPARISON TO OTHER APPROACHES

Comparing sensors based on different approaches, involving different output and input variables, is not in general an easy task. Nevertheless, we will give some comparative data between the proposed sensor and those reported in the literature, devoted to the measurement of diluted concentrations of liquid solutions and to the determination of the complex permittivity of liquids.

Concerning solute content measurement, Babajanyan [36] report microwave sensors for the measurement of sodium chloride, whereas in [37]–[41] the objective is the determination of glucose concentration. The maximum

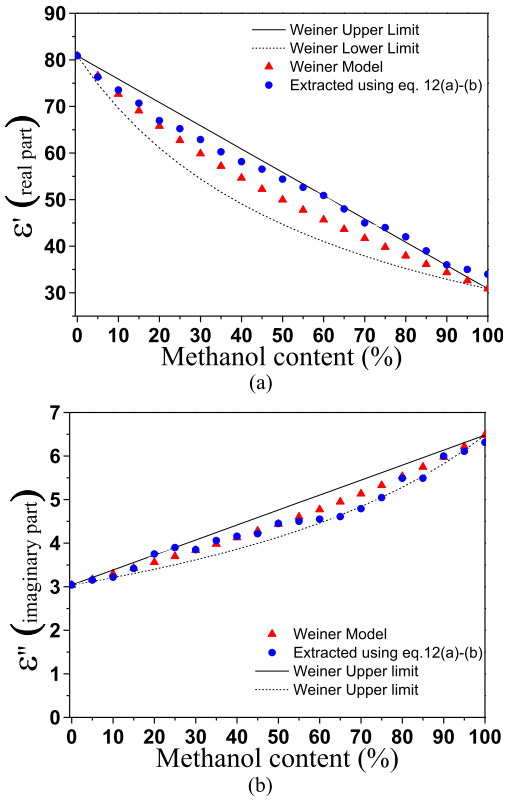

FIGURE 19. Extracted value for the real (a) and imaginary (b) parts of the complex dielectric constant in mixtures of DI water/methanol. The static Weiner model is also included for comparison purposes.

TABLE 3. Comparison of various microwave fluidic sensors for solute concentration measurement in liquid solutions.

Ref.	*Max. sensitivity* (dB/g/L)	*Resolution* (g/L)	*Dynamic range* (g/L)
[36]	0.005	2	10
[37]	0.003	1	300
[38]	1.75	1.5	5.5
[39]	0.017	10	150
[40]	0.003	5	300
This work	**4.3**	**0.25**	**80**

sensitivity and resolution in these sensors are given in Table 3, together with the values extracted from our sensing device. It can be seen that the sensor proposed in this paper is able to detect concentrations of sodium in DI water as small as 0.25g/L, which is a value by far smaller than the other values reported in the table. Concerning the sensitivity, the device of [38] exhibits a good sensitivity as compared to those of [36], [37], [39], and [40] but the sensor reported in this work exhibits much superior sensitivity. The reported input dynamic range of the proposed sensor is 80 g/L, which is a very wide dynamic range for solute concentration measurements in diluted solutions.

Concerning the measurement of the complex permittivity of liquids (particularly mixtures of DI water and ethanol) using resonant elements [5], [31], [42]–[45], the performance of the different sensors is compared in Table 4, which is an extended table with regard to the one reported in [31] (Table 2 of that article). S_{av} is the average frequency sensitivity of the dielectric constant, whereas $S_{av,f}$ is the previous sensitivity divided by the central frequency, f_0, of the frequency span, as defined in [31]. This latter sensitivity is the one that should be compared, due to the different frequency operations of the different sensors. In Table 4, the minimum detectable fractional volume, F_v, is another relevant parameter. It can be seen that the sensor proposed in [45] exhibits an extremely good resolution and very good normalized sensitivity. It is able to discriminate 50 ppm of ethanol in DI water, although with resonance shifts smaller than 1 MHz. Indeed, in the sensor proposed in this work, the minimum considered volume fraction of ethanol has been considered to be $F_v = 5\%$, since the focus has been oriented on obtaining the complex dielectric constant of liquids with reasonable accuracy, and this has been achieved to the light of Fig. 19, where the measured complex dielectric constant of mixtures of methanol has been reasonably predicted. On the other hand, it is worth mentioning that the proposed sensor, mainly based on the variation of the magnitude of the insertion loss, exhibits high sensitivity of $\Delta|S_{21}^{DC}|_{\max}$ to the ethanol (or methanol) content, as can be seen in Figs. 15 and 18, and, consequently, it should be able to resolve variations of ethanol (or methanol) concentration smaller than 5%.

TABLE 4. Comparison of various DI water/ethanol microwave fluidic sensors.

Reference	f_0 (GHz)	S_{av} (MHz)	$S_{av,f}$ (%)	F_v (%)
[42]	20	59.75	2.98	5
[5]	2	4.76	2.38	10
[43]	1.9	1.53	0.81	10
[44]	3.5	9.16	2.61	10
[31]	0.87	0.79	0.91	10
[45]	2.5	8	3.2	0.005
This work	**0.9**	**1.8**	**1.86**	**5**

It should be noted that we have carried out the measurements by means of a 4-port vector network analyzer (VNA). An alternative to simplify the measurement set-up (representing also a reduction in costs) is to use a 2-port VNA. Since the OCSRR-loaded lines of the sensor are uncoupled, we can simply measure the transmission coefficient of the reference channel line, and then the transmission coefficient of the LUT channel line as many times as different LUT samples are considered. Then, by using (1), the cross-mode transmission coefficient can be inferred. The use of a pair of switches to connect the VNA either to the reference or channel line can be also considered. As long as switches are inexpensive and there are commercially available low-cost portable 2-port VNAs, the cost of the sensor structure may be reasonable and comparable to other similar sensing approaches.

To end this section, we would like to emphasize that the main contribution/originality of this work (as compared to previous similar works by Vélez *et al.* [28], [31]) is the method for the measurement of solution concentration and dielectric characterization in liquids, based on the measurement of the cross-mode transmission coefficient.

This parameter is very sensitive to small perturbations (asymmetries) between the reference channel and the LUT channel, and allows us for the detection of small concentrations of solute (Na in our case) in DI water, as revealed in Table 3. It also provides good performance with regard to the characterization of the complex dielectric constant of liquids, as can be seen in the comparative Table 4. Indeed, we introduced this sensing method in [28] for the first time. However, it was not applied to the measurement of solute concentration or to the dielectric characterization of liquids (the validation in [28] was simply carried out by perturbing the dimensions of one of the OCSRRs with regard to the other one).

As compared to the work in [31], in that paper we also report results related to the dielectric characterization of liquids (mixtures of DI water and ethanol), but the sensing method is very different. In [31], a splitter/combiner configuration and a pair of split ring resonators were used, and the sensing principle relies on the pair of notches that are generated when the reference liquid and the LUT are different (frequency splitting). As compared to [31], the method reported in the present paper is more sensitive, as can be appreciated in table 4, and it is able to resolve smaller volume fractions of ethanol. Although the results in Fig. 16 look similar to those of Fig. 13 of [31], the sensing method is completely different, and better sensing performance has been obtained in the sensor reported in this paper.

VI. CONCLUSION

In conclusion, a new type of microwave sensors based on a pair of symmetric uncoupled lines, each one loaded with an OCSRR, has been proposed and applied to the measurement of solute concentration in liquid solutions, and to the measurement of the complex dielectric constant in liquids. For these purposes, fluidic channels have been added on top of both OCSRRs. The sensing principle is based on the measurement of the cross-mode insertion loss, very sensitive to small perturbations between the reference liquid, injected in one of the channels, and the liquid under test (LUT), injected to the other channel. The proposed sensor has been used to determine sodium concentration in DI water, and it has been demonstrated that the sensor exhibits excellent sensitivity and it is able to detect sodium concentrations as small as 0.25 g/L. For dielectric characterization of liquids, the functionality has been validated by measuring the complex dielectric constant of solutions of methanol in DI water, whereas mixtures of DI water and ethanol have been used for calibration purposes. Additionally, a sensitivity analysis, based on the equivalent circuit model of the proposed sensor and valid for small perturbations, has been carried out. From this analysis, interesting design guidelines for sensor design have been inferred.

REFERENCES

[1] F. Martín, F. Falcone, J. Bonache, R. Marqués, and M. Sorolla, "Split ring resonator-based left-handed coplanar waveguide," *Appl. Phys. Lett.*, vol. 83, no. 22, pp. 4652–4654, Dec. 2003.

[2] F. Falcone, T. Lopetegi, J. D. Baena, R. Marqués, F. Martín, and M. Sorolla, "Effective negative-ε stopband microstrip lines based on complementary split ring resonators," *IEEE Microw. Wireless Compon. Lett.*, vol. 14, no. 6, pp. 280–282, Jun. 2004.

[3] M. Puentes, C. Weiß, M. Schüßler, and R. Jakoby, "Sensor array based on split ring resonators for analysis of organic tissues," in *IEEE MTT-S Int. Microw. Symp. Dig.*, Baltimore, MD, USA, Jun. 2011, pp. 1–4.

[4] M. P. Vargas, *Planar Metamaterial Based Microwave Sensor Arrays for Biomedical Analysis and Treatment*. Berlin, Germany: Springer, 2014.

[5] A. Ebrahimi, W. Withayachumnankul, S. Al-Sarawi, and D. Abbott, "High-sensitivity metamaterial-inspired sensor for microfluidic dielectric characterization," *IEEE Sensors J.*, vol. 14, no. 5, pp. 1345–1351, May 2014.

[6] M. Schueler, C. Mandel, M. Puentes, and R. Jakoby, "Metamaterial inspired microwave sensors," *IEEE Microw. Mag.*, vol. 13, no. 2, pp. 57–68, Mar. 2012.

[7] M. S. Boybay and O. M. Ramahi, "Material characterization using complementary split-ring resonators," *IEEE Trans. Instrum. Meas.*, vol. 61, no. 11, pp. 3039–3046, Nov. 2012.

[8] C.-S. Lee and C.-L. Yang, "Complementary split-ring resonators for measuring dielectric constants and loss tangents," *IEEE Microw. Wireless Compon. Lett.*, vol. 24, no. 8, pp. 563–565, Aug. 2014.

[9] C.-L. Yang, C.-S. Lee, K.-W. Chen, and K.-Z. Chen, "Noncontact measurement of complex permittivity and thickness by using planar resonators," *IEEE Trans. Microw. Theory Techn.*, vol. 64, no. 1, pp. 247–257, Jan. 2016.

[10] A. K. Horestani, J. Naqui, Z. Shaterian, D. Abbott, C. Fumeaux, and F. Martín, "Two-dimensional alignment and displacement sensor based on movable broadside-coupled split ring resonators," *Sens. Actuators A, Phys.*, vol. 210, pp. 18–24, Apr. 2014.

[11] J. Naqui, C. Damm, A. Wiens, R. Jakoby, L. Su, and F. Martín, "Transmission lines loaded with pairs of magnetically coupled stepped impedance resonators (SIRs): Modeling and application to microwave sensors," in *IEEE MTT-S Int. Microw. Symp. Dig.*, Tampa, FL, USA, Jun. 2014, pp. 1–4.

[12] L. Su, J. Naqui, J. Mata-Contreras, and F. Martín, "Modeling metamaterial transmission lines loaded with pairs of coupled split ring resonators," *IEEE Antennas Wireless Propag. Lett.*, vol. 14, pp. 68–71, 2015.

[13] L. Su, J. Naqui, J. Mata, and F. Martín, "Dual-band epsilon-negative (ENG) transmission line metamaterials based on microstrip lines loaded with pairs of coupled complementary split ring resonators (CSRRs): Modeling, analysis and applications," in *Proc. 9th Int. Congr. Adv. Electromagn. Mater. Microw. Opt. (METAMATERIALS)*, Oxford, U.K., Sep. 2015, pp. 7–12.

[14] L. Su, J. Naqui, J. Mata-Contreras, P. Vélez, and F. Martín, "Transmission line metamaterials based on pairs of coupled split ring resonators (SRRs) and complementary split ring resonators (CSRR): A comparison to the light of the lumped element equivalent circuits," in *Proc. Int. Conf. Electromagn. Adv. Appl. (ICEAA)*, Torino, Italy, Sep. 2015, pp. 7–11.

[15] L. Su, J. Naqui, J. Mata-Contreras, and F. Martín, "Modeling and applications of metamaterial transmission lines loaded with pairs of coupled complementary split ring resonators (CSRRs)," *IEEE Antennas Wireless Propag. Lett.*, vol. 15, pp. 154–157, 2016.

[16] L. Su, J. Mata-Contreras, P. Vélez, and F. Martín, "Splitter/combiner microstrip sections loaded with pairs of complementary split ring resonators (CSRRs): Modeling and optimization for differential sensing applications," *IEEE Trans. Microw. Theory Techn.*, vol. 64, no. 12, pp. 4362–4370, Dec. 2016.

[17] J. Naqui, M. Durán-Sindreu, and F. Martín, "Novel sensors based on the symmetry properties of split ring resonators (SRRs)," *Sensors*, vol. 11, no. 8, pp. 7545–7553, 2011.

[18] F. Martín, *Artificial Transmission Lines for RF and Microwave Applications*. Hoboken, NJ, USA: Wiley, 2015.

[19] J. Naqui, *Symmetry Properties in Transmission Lines Loaded With Electrically Small Resonators: Circuit Modeling and Applications*. Berlin, Germany: Springer, 2016.

[20] J. Naqui, M. Durán-Sindreu, and F. Martín, "Alignment and position sensors based on split ring resonators," *Sensors*, vol. 12, no. 9, pp. 11790–11797, Aug. 2012.

[21] A. K. Horestani, C. Fumeaux, S. F. Al-Sarawi, and D. Abbott, "Displacement sensor based on diamond-shaped tapered split ring resonator," *IEEE Sensors J.*, vol. 13, no. 4, pp. 1153–1160, Apr. 2013.

[22] A. K. Horestani, D. Abbott, and C. Fumeaux, "Rotation sensor based on horn-shaped split ring resonator," *IEEE Sensors J.*, vol. 13, no. 8, pp. 3014–3015, Aug. 2013.

[23] J. Naqui and F. Martín, "Transmission lines loaded with bisymmetric resonators and their application to angular displacement and velocity sensors," *IEEE Trans. Microw. Theory Techn.*, vol. 61, no. 12, pp. 4700–4713, Dec. 2013.
[24] J. Naqui and F. Martín, "Angular displacement and velocity sensors based on electric-LC (ELC) loaded microstrip lines," *IEEE Sensors J.*, vol. 14, no. 4, pp. 939–940, Apr. 2014.
[25] A. K. Horestani, J. Naqui, D. Abbott, C. Fumeaux, and F. Martín, "Two-dimensional displacement and alignment sensor based on reflection coefficients of open microstrip lines loaded with split ring resonators," *Electron. Lett.*, vol. 50, no. 8, pp. 620–622, Apr. 2014.
[26] J. Naqui and F. Martín, "Microwave sensors based on symmetry properties of resonator-loaded transmission lines," *J. Sensors*, vol. 2015, Jan. 2015, Art. no. 741853.
[27] J. Naqui, J. Coromina, A. Karami-Horestani, C. Fumeaux, and F. Martín, "Angular displacement and velocity sensors based on coplanar waveguides (CPWs) loaded with S-shaped split ring resonators (S-SRR)," *Sensors*, vol. 15, no. 5, pp. 9628–9650, 2015.
[28] P. Vélez, L. Su, J. Mata-Contreras, F. Martín, K. Grenier, and D. Dubuc, "Modeling and analysis of pairs of open complementary split ring resonators (OCSRRs) for differential permittivity sensing," in *IEEE MTT-S Int. Microw. Symp. Dig., Adv. Mater. Process. RF THz Appl. (IMWS-AMP)*, Pavia, Italy, Sep. 2017, pp. 20–22.
[29] L. Su, J. Mata-Contreras, P. Vélez, and F. Martín, "Estimation of conductive losses in complementary split ring resonator (CSRR) loading an embedded microstrip line and applications," in *IEEE MTT-S Int. Microw. Symp. Dig.*, Honolulu, HI, USA, Jun. 2017, pp. 476–479.
[30] L. Su, J. Mata-Contreras, P. Vèlez, and F. Martín, "Estimation of the complex permittivity of liquids by means of complementary split ring resonator (CSRR) loaded transmission lines," in *IEEE MTT-S Int. Microw. Symp. Dig. Adv. Mater. Process. (IMWS-AMP)*, Pavia, Italy, Sep. 2017, pp. 20–22.
[31] P. Vélez, L. Su, K. Grenier, J. Mata-Contreras, D. Dubuc, and F. Martín, "Microwave microfluidic sensor based on a microstrip splitter/combiner configuration and split ring resonators (SRRs) for dielectric characterization of liquids," *IEEE Sensors J.*, vol. 17, no. 20, pp. 6589–6598, Oct. 2017.
[32] A. Ebrahimi, J. Scott, and K. Ghorbani, "Differential sensors using microstrip lines loaded with two split-ring resonators," *IEEE Sensors J.*, vol. 18, no. 14, pp. 5786–5793, Jul. 2018.
[33] J. Mata-Contreras, C. Herrojo, and F. Martín, "Application of split ring resonator (SRR) loaded transmission lines to the design of angular displacement and velocity sensors for space applications," *IEEE Trans. Microw. Theory Techn.*, vol. 65, no. 11, pp. 4450–4460, Nov. 2017.
[34] A. Velez, F. Aznar, J. Bonache, M. C. Velazquez-Ahumada, J. Martel, and F. Martin, "Open complementary split ring resonators (OCSRRs) and their application to wideband CPW band pass filters," *IEEE Microw. Wireless Compon. Lett.*, vol. 19, no. 4, pp. 197–199, Apr. 2009.
[35] O. Weiner, "Die theorie des Mischkorpers fur das feld der statonare Stromung i. Die mittelwertsatze fur kraft, polarisation und energie," *Trans. Math.-Phys. Class Roy. Saxon Soc. Sci.*, vol. 32, pp. 509–604, 1912.
[36] A. Babajanyan, J. Kim, S. Kim, K. Lee, and B. Friedman, "Sodium chloride sensing by using a near-field microwave microprobe," *Appl. Phys. Lett.*, vol. 89, no. 18, p. 183504, 2006.
[37] A. Bababjanyan, H. Melikyan, S. Kim, J. Kim, K. Lee, and B. Friedman, "Real-time noninvasive measurement of glucose concentration using a microwave biosensor," *J. Sensors*, vol. 2010, Dec. 2010, Art. no. 452163.
[38] S. Kim *et al.*, "Noninvasive *in vitro* measurement of pig-blood D-glucose by using a microwave cavity sensor," *Diabetes Res. Clin. Pract.*, vol. 96, no. 3, pp. 379–384, 2012.
[39] N. Sharafadinzadeh, M. Abdolrazzaghi, and M. Daneshmand, "Highly sensitive microwave split ring resonator sensor using gap extension for glucose sensing," in *IEEE MTT-S Int. Microw. Symp. Dig. Adv. Mater. Process. (IMWS-AMP)*, Pavia, Italy, Sep. 2017, pp. 20–22.
[40] J. Kim, A. Babajanyan, A. Hovsepyan, K. Lee, and B. Friedman, "Microwave dielectric resonator biosensor for aqueous glucose solution," *Rev. Sci. Instrum.*, vol. 79, no. 8, p. 086107, 2008.
[41] A. Ebrahimi, W. Withayachumnankul, S. F. Al-Sarawi, and D. Abbott, "Microwave microfluidic sensor for determination of glucose concentration in water," in *Proc. IEEE 15th Medit. Microw. Symp. (MMS)*, Lecce, Italy, Nov./Dec. 2015, pp. 1–3.
[42] T. Chretiennot, D. Dubuc, and K. Grenier, "A microwave and microfluidic planar resonator for efficient and accurate complex permittivity characterization of aqueous solutions," *IEEE Trans. Microw. Theory Techn.*, vol. 61, no. 2, pp. 972–978, Feb. 2013.
[43] W. Withayachumnankul, K. Jaruwongrungsee, A. Tuantranont, C. Fumeaux, and D. Abbott, "Metamaterial-based microfluidic sensor for dielectric characterization," *Sens. Actuators A, Phys.*, vol. 189, pp. 233–237, Jan. 2013.
[44] A. Salim and S. Lim, "Complementary split-ring resonator-loaded microfluidic ethanol chemical sensor," *Sensors*, vol. 16, no. 11, pp. 1–13, 2016.
[45] M. Abdolrazzaghi, M. Daneshmand, and A. K. Iyer. (2017). "Strongly enhanced sensitivity in planar microwave sensors based on metamaterial coupling." [Online]. Available: https://arxiv.org/abs/1709.02364

PARIS VÉLEZ (S'10–M'14) was born in Barcelona, Spain, in 1982. He received the bachelor's degree in telecommunications engineering, specializing in electronics, the master's degree in electronics engineering, and the Ph.D. degree in electrical engineering, with a thesis Common Mode Suppression Differential Microwave Circuits Based on Metamaterial Concepts and Semilumped Resonators, from the Universitat Autònoma de Barcelona in 2008, 2010, and 2014, respectively. During the Ph.D. degree, he received the Pre-Doctoral Teaching Fellowship and the Research Fellowship by the Spanish Government from 2011 to 2014. Actually, his scientific activity is focused on the miniaturization of passive circuits RF/microwave-based metamaterials. He is a Reviewer of the IEEE T-MTT and of other journals.

KATIA GRENIER (S'99–M'03) received the M.S. and Ph.D. degrees in electrical engineering from the University of Toulouse, Toulouse, France, in 1997 and 2000, respectively. She was involved in microelectromechanical systems circuits on silicon. She was a Post-Doctoral Fellow of Agere Systems (Bell Labs). In 2001, she joined the Laboratory of Analysis and Architecture of System, National Scientific Research Center (LAAS-CNRS), Université de Toulouse, Toulouse. From 2007 to 2009, she was with the Laboratory for Integrated Micromechatronic Systems, CNRS, Institute of Industrial Science, The Universtity of Tokyo, Tokyo, Japan, where she was involved in launching research activities on microwave-based biosensors. Her research interests with LAAS-CNRS are now focused on the development of fluidic-based microsystems, notably for biological and medical applications at the cellular and molecular levels. She is a member of the IEEE MTT-10 Technical Committee on Biological Effect and Medical Applications of RF and Microwave, IEEE Microwave Theory and Techniques Society.

JAVIER MATA-CONTRERAS was born in Málaga, Spain, in 1976. He received the Ingeniería de Telecomunicación degree and the Ph.D. degree with a thesis Distributed Amplifiers and Mixers With Transmission Lines Based on Metamaterials from the Universidad de Málaga (UMA), in 2000 and 2010, respectively. In 2000, he joined the Department of Ingeniería de Comunicaciones, UMA, as an Assistant Professor. He is currently with CIMITEC and the Universitat Autònoma de Barcelona as a Visiting Professor. His research interests include active and passive microwave devices, and active distributed circuits based on metamaterials, among others.

DAVID DUBUC (S'99–M'03) received the Agrégation degree from the École Normale Supérieure de Cachan, Paris, France, in 1996, and the M.S. and Ph.D. degrees in electrical engineering from the Université de Toulouse, Toulouse, France, in 1997 and 2001, respectively. From 2002 to 2013, he was an Associate Professor with the Université de Toulouse, and a Researcher with the Laboratory of Analysis and Architecture of System, National Scientific Research Center (CNRS), Toulouse. From 2007 to 2009, he was a Visiting Senior Researcher with the Laboratory of Integrated Micromechatronic Systems, CNRS, Institute of Industrial Science, The University of Tokyo, Tokyo, Japan. Since 2013, he has been a Professor with the Université de Toulouse. His research interests include the development of microwave circuits integrated due to microtechnologies and their applications to wireless telecommunication and biology.

FERRAN MARTÍN (M'04–SM'08–F'12) was born in Barakaldo, Vizcaya, Spain, in 1965. He received the B.S. degree in physics and the Ph.D. degree from the Universitat Autònoma de Barcelona (UAB) in 1992 and 1988, respectively. From 1994 to 2006, he was an Associate Professor in electronics with the Departament d'Enginyeria Electrònica, UAB, and since 2007, he has been a Full Professor of electronics. In recent years, he has been involved in different research activities, including the modeling and simulation of electron devices for high-frequency applications, millimeter-wave and THz generation systems, and the application of electromagnetic bandgaps to microwave and millimeter-wave circuits. He is currently very active in the field of metamaterials and their applications to the miniaturization and optimization of microwave circuits and antennas. He is also the Head of the Microwave Engineering, Metamaterials and Antennas Group (GEMMA Group), UAB, and the Director of CIMITEC, a Research Center on Metamaterials supported by TECNIO (Generalitat de Catalunya). He has authored or co-authored over 500 technical conference, letter, journal papers, and book chapters. He has co-authored the book on metamaterials *Metamaterials with Negative Parameters: Theory, Design and Microwave Applications* (John Wiley & Sons Inc., 2008). He has authored the book *Artificial Transmission Lines for RF and Microwave Applications* (John Wiley & Sons Inc., 2015). He has generated 17 Ph.D. students. He has filed several patents on metamaterials. He was the head of several development contracts. He is a member of the IEEE Microwave Theory and Techniques Society, the Technical Committees of the European Microwave Conference, and the International Congress on Advanced Electromagnetic Materials in Microwaves and Optics (Metamaterials). He has been a fellow of IET since 2016. Among his distinctions, he has received the 2006 Duran Farell Prize for technological research. He was a recipient of two ICREA ACADEMIA Awards (in 2008 and 2013). He has organized several international events related to metamaterials, including workshops at the IEEE International Microwave Symposium (in 2005 and 2007) and the European Microwave Conference (2009), and the Fifth International Congress on Advanced Electromagnetic Materials in Microwaves and Optics (Metamaterials 2011), where he has acted as the Chair of the Local Organizing Committee. He is currently the Parc de Recerca UAB-Santander Technology Transfer Chair. He is a Reviewer of the IEEE TRANSACTIONS ON MICROWAVE THEORY AND TECHNIQUES and the IEEE MICROWAVE AND WIRELESS COMPONENTS LETTERS, among many other journals. He serves as a member for the Editorial Board of *IET Microwaves, Antennas and Propagation* and the *International Journal of RF and Microwave Computer-Aided Engineering*. He has acted as a Guest Editor of three special issues on *Metamaterials* in three international journals.